analytical chemistry

pubs.acs.org/ac Article

Rolling Circle Amplification-Coupled Glass Nanopore Counting of Mild Traumatic Brain Injury-Related Salivary miRNAs

Ming Dong, Zifan Tang, Steven Hicks, and Weihua Guan*

Cite This: *Anal. Chem.* 2022, 94, 3865−3871 Read Online

ACCESS | Metrics & More | Article Recommendations | Supporting Information

ABSTRACT: Mild traumatic brain injury (mTBI) could be underdiagnosed and underreported due to the delayed onset of symptoms and the conventional subjective assessment. Recent studies have suggested that salivary microRNAs (miRNAs) could be reliable biomarkers for objective mTBI diagnosis. In this work, we demonstrated a rolling circle amplification (RCA)-coupled resistive pulse-counting platform for profiling mTBI-related miRNAs, using easy-to-fabricate large glass nanopores (200 nm diameter). The method relies on the linear and specific elongation of the miRNA to a much larger RCA product, which the large glass nanopore can digitally count with a high signal-to-noise ratio. We developed and validated the RCA assay against let-7a, miR-30e, and miR-21. We demonstrated the quantification capability of this large glass nanopore counting platform for purified miRNAs as well as miRNAs in salivary total RNA background. Finally, we quantitatively evaluated the performance of profiling each individual miRNAs in a mixed analyte. Our results showed that the RCA-coupled large glass nanopore counting provides a promising and accessible alternative toward the clinical diagnosis of mTBI using salivary miRNAs.

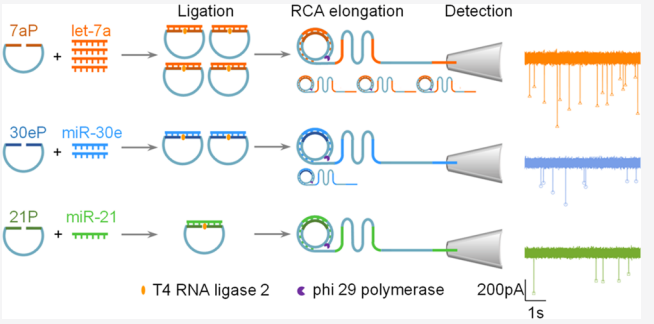

Downloaded via Weihua Guan on March 10, 2022 at 01:49:43 (UTC).
See https://pubs.acs.org/sharingguidelines for options on how to legitimately share published articles.

Mild traumatic brain injury (mTBI), or concussion, is the most common type of traumatic brain injury.[1] mTBI symptoms include headaches, fatigue, depression, anxiety, and irritability as well as impaired cognitive function. Yet it is well known that mTBI is both underdiagnosed and underreported due to delayed onset of symptoms and conventional subjective assessment methods like cognitive testing and symptom scale.[1] Objective, rapid, and accurate mTBI diagnosis remains an unmet need for effectively managing mTBI. Several technologies for objective mTBI diagnosis have been proposed, including neuroimaging,[2] electrophysiology,[3] and blood biomarkers.[4] However, these existing technologies were not without challenges. For example, while changes in proteins and lipids in the blood were used to determine the risk of intracranial bleeding, most mTBIs do not result in intracranial bleeding.[5] Besides, those blood biomarkers are typically present at low concentrations (fM to pM), are susceptible to degradation, and may have difficulty crossing the blood−brain barrier in cases of mTBIs.[6] On the other hand, neuroimaging and electrophysiology require expensive equipment and specialist interpretation.[2] The long turnaround time and complex workflow of these existing technologies preclude their adoption for rapid diagnosis of the mTBI, particularly at the point-of-care testing.

Recent findings have suggested that salivary microRNAs (miRNAs) are promising biomarkers for mTBI diagnosis based on their varied expression levels.[7] miRNAs are small single-stranded non-coding molecules that function in RNA silencing and post-transcriptional regulation of gene expression.[8] Because the saliva can be obtained non-invasively, salivary miRNA represents an ideal biomarker for rapid mTBI diagnosis. However, detecting and differentiating miRNAs is challenging due to their short length and high homogeneity.[9] The common techniques for miRNA profiling include northern blotting,[10] RT-PCR,[11] microarrays,[12] and next-generation sequencing (NGS).[13] While readily available and effective, these methods fall short of the requirement for rapid, inexpensive, and accurate miRNA profiling for mTBI diagnosis. For instance, northern blotting has a complex workflow and requires a radioactive label.[14] The primer efficacy in RT-PCR and the hybridization in microarrays are limited by the short length of miRNA. The turnaround time and the cost of NGS are still prohibitive for routine clinical adoption.[13] To the end of rapid and accessible mTBI diagnosis using salivary miRNAs, alternative approaches have been investigated, such as nanoparticle-derived probes,[15] electrochemical methods,[16] and isothermal amplification.[17] Among them, rolling circle amplification (RCA) is one of the isothermal methods to

Received: November 3, 2021
Accepted: February 14, 2022
Published: February 22, 2022

© 2022 American Chemical Society

https://doi.org/10.1021/acs.analchem.1c04781
Anal. Chem. 2022, 94, 3865−3871

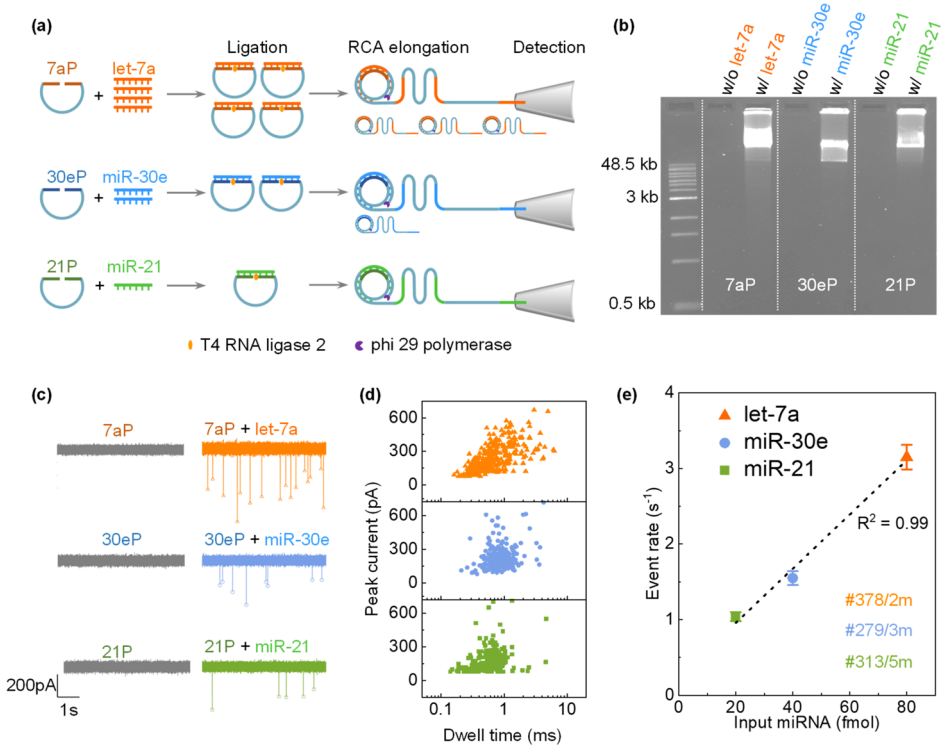

Figure 1. (a) Schematics of the RCA-based miRNA detection method. 7aP, 30eP, and 21P denote the padlock probe for let-7a, miR-30e, and miR-21, respectively. The orange region of 7aP, blue region of 30eP, and green region of 21P are complementary to let-7a, miR-30e, and miR-21, respectively. (b) Gel image of RCA products. (c) Representative current traces for RCA reactions with probes only and for RCA reactions with both padlock probes and the target miRNA. (d) Distribution of dwell time and peak current for blockage events. (e) Measured event rate as a function of the input miRNA concentration. ("#378/2m" means that 378 events were observed in 2 min measurement; the error bars represent the Poisson counting uncertainty $n^{1/2}/T$.)

detect miRNAs with relatively short turnaround time and simple workflow. Due to the specificity required by the hybridization and ligation process, even one nucleotide difference in miRNA can be discriminated via RCA assay.[18]

While both solid-state[19] and biological[20] nanopores have been previously used to detect/quantify miRNA, these methods require fine control over the nanopore size (less than 5 nm). Here, we demonstrated an RCA-coupled glass nanopore counting platform for profiling a panel of mTBI-related miRNAs, using easy-to-fabricate large glass nanopores (200 nm diameter). Due to the specificity of the RCA assay, only target miRNA could be specifically elongated to a long single-stranded DNA (ssDNA) product, which the large glass nanopore can count with a high signal-to-noise ratio. The linearity between the ssDNA RCA product and the input miRNA made the quantification of miRNAs possible. We demonstrated that the RCA-coupled glass nanopore counting platform could work with the salivary total RNA background. This method could be easily scaled up to accommodate more panel members thanks to the scalability of the electronic platform. The findings in this study provide a promising alternative approach for analyzing miRNAs using nanopore sensors.

EXPERIMENTAL SECTION

Materials and Chemicals. RNAs and DNAs were synthesized by integrated DNA technologies; the detailed sequences are listed in Table S1. Nuclease-free molecular biology-grade water was from NEB (B1500S). DNA gel blue loading dye (6×, B7021S) was from NEB. Agarose was from Fisher Scientific (BP160100). DNA ladder was from NEB (N3239S). SYBR Gold nucleic acid gel stain (S11494) was from NEB. Deoxynucleotide solution mix, T4 RNA ligase 2, and Phi29 DNA polymerase were purchased from NEB. The salivary total RNA was extracted using a ChargeSwitch total RNA cell kit from Invitrogen. Ag/AgCl electrodes were house-made with 0.375 mm Ag wires (Warner Instruments, Hamden, USA). Potassium chloride and 1× Tris-EDTA buffer solution (10 mM Tris-HCl, 1 mM disodium EDTA, pH 8.0) were purchased from Sigma-Aldrich. The solution was filtered with a 0.2 μm Anotop filter (Whatman) and degassed in a vacuum chamber prior to use.

Rolling Circle Amplification Assay. For the ligation reactions, the reaction mixture consisted of nuclease-free water, ligation buffer [50 mM Tris-HCl, pH 7.5, 2 mM $MgCl_2$, 10 mM dithiothreitol (DTT), 400 mM ATP], 2 U of T4 RNA ligase 2, 160 fmol padlock probes unless otherwise stated, and the target miRNAs (single miRNA or miRNA mixtures) in a reaction volume of 10 μL. Before the ligase and ligation buffer were added, the reaction mixture was heated at 55 °C for 5 min and annealed to 39 °C at −1 °C/min in the C1000 Touch Thermal Cycler (Bio-Rad, USA). The ligase and the buffer were then added, and the reaction mixture was incubated at 39 °C for 45 min. The products of the ligation reaction were added to the 10 μL RCA reaction mixture containing 80 mM Tris-HCl (pH 7.5), 100 mM KCl, 20 mM $MgCl_2$, 10 mM $(NH_4)_2SO_4$, 8 mM DTT, 500 mM of each deoxynucleoside triphosphate (dNTP), and 20 U of phi29 DNA polymerase. The RCA reactions were performed at 30 °C for 30 min.

https://doi.org/10.1021/acs.analchem.1c04781
Anal. Chem. 2022, 94, 3865−3871

Gel Analysis. The reaction mixture for gel electrophoresis was terminated by adding 4 μL gel blue loading dye, and the 1.0% agarose gel (made with 1× Tris-borate-EDTA (TBE) buffer) was kept running for 1 h at 120 V. After that, the SYBR Gold nucleic acid gel stain was used to stain the gel for 30 min. Gel electrophoresis images were acquired with a GelDoc Go imaging system (Bio-Rad, USA).

Salivary Total RNA Extraction. The saliva samples were collected from healthy volunteers. The total RNA was extracted from 1 mL saliva by a ChargeSwitch total RNA cell kit following the protocol. The isolated total RNA was eluted with 75 μL elution buffer. The final concentration of the extracted RNA was measured by NanoDrop 2000 (Thermo Fisher Scientific) as 9.6 ng/μL. The synthetic let-7a was spiked into 7 μL extracted saliva RNA solution at various quantities ranging from 10 to 160 fmol.

Glass Nanopore Fabrication. The quartz capillaries (QF120-90-7.5; Sutter Instrument Co, USA) were cleaned by piranha for 30 min to remove organic contaminants, then rinsed with DI water, and dried in the oven at 100 °C for 30 min. The capillaries were oxygen plasma cleaned for 5 min to enhance the hydrophilic property. The capillary was then pulled by a laser pipet puller (P-2000, Sutter Instrument, USA) using a two-line program: (1) heat 575, filament 3, velocity 35, delay 145, and pull 75; (2) heat 425, filament 0, velocity 15, delay 128, and pull 185. This recipe typically produced pores with a diameter of 217 ± 9 nm. The SEM image and electrical properties of a typical pore are shown in Figure S1. Due to the influence of humidity and temperature, the pulling parameters should be modified accordingly. After pulling, the capillary was filled with Tris-EDTA buffered 1 M KCl solution immediately using a micro-injector.

Nanopore Sensing and Data Analysis. The 20 μL RCA reaction mixture for nanopore sensing was terminated by adding 80 μL Tris-EDTA buffered 1.25 M KCl solution to form 100 μL of the testing sample. The 1 M KCl-filled glass pore was fixed by a pipette holder and immersed in the PCR tube containing the 100 μL testing sample. Ag/AgCl electrodes were placed inside the glass capillary as well as in the test sample solution. A typical voltage of 400 mV was applied across the pore by a 6363 DAQ card (National Instruments, USA). A trans-impedance amplifier (Axopatch 200B, Molecular Devices, USA) was used to amplify the resulting current and then digitized by the 6363 DAQ card at 100 kHz sampling rate. Finally, a customized MATLAB (MathWorks) software was used to analyze the current time trace and extract the single-molecule translocation information. The threshold of the event peak was set at 5 times of the standard deviation of the current traces. If clogging was observed, 5 times *IV* sweeps from −500 to 500 mV were applied to restore the pore.

RESULTS AND DISCUSSION

Principle Validation. Figure 1a shows the principle of the RCA-coupled glass nanopore counting of miRNAs. Recent studies have shown that miRNA expression levels could be up-regulated after mTBI. We chose a subset of panels from previous works in this study: let-7a (65% increased),[21] miR-30e (88% increased),[22] and miR-21 (280% increased).[23,24] Padlock probes[18] were designed to specifically target the let-7a, miR-30e, and miR-21 (see Table S1 for the detailed probe design). As shown, the miRNA first binds to its specific probe. The hybridized complex is further ligated by the T4 RNA ligase 2 to form a closed circular structure. After that, the phi29 DNA polymerase is introduced to elongate the hybridized miRNA using the probe as a template (RCA elongation). The RCA elongation process produces a long ssDNA product greater than 70k nucleotides.[25] This ssDNA product can be easily detected by the glass sub-micron pore with a high signal-to-noise ratio due to its large size. In contrast, small molecules like miRNAs and probes cannot be detected. The event rate of products is counted through the nanopore without sizing by event shape. This is because the RCA products themselves could have a size distribution, and products could conform during translocation. By measuring the concentration of the enlarged ssDNA product through the event rate,[26] one can determine the initial miRNA concentrations because the quantity of the initial miRNA molecule is linear with the number of elongated ssDNA products.

Prior to the glass nanopore quantification experiment, we first validated the RCA assay for let-7a, miR-30e, and miR-21 (see the Experimental Section for details). As shown in the gel results (Figure 1b), reactions without the miRNA input (i.e., with probes only) produced no elongated product, whereas reactions with miRNAs showed the product with a length much larger than 48.5 kb. This confirmed that let-7a, miR-30e, and miR-21 can be successfully elongated to their corresponding ssDNA products through the RCA reaction.

After confirming that indeed ssDNA amplicons were produced, we went on to test these amplicon solutions with the glass sub-micron pore sensor. A typical glass pore used in our experiment was about 200 nm in diameter (Figure S1). We intentionally used this large pore to avoid signals generated by small molecules like miRNAs and padlock probes. We applied a voltage of 400 mV across the pore and counted the translocation events by monitoring the ionic current. The nanopore counting was conducted until at least 250 events were captured to reduce the event rate uncertainty (≤6%)[26] or 10 min were reached. As shown in the time traces in Figure 1c, for the probe-only reactions (three left traces), no events were observed during the 5 s of the measurement. In fact, for a longer measurement of 10 min, less than 5 events could be observed (Figure S2), indicating that the background event rate was less than 0.008 s^{-1}. This negligible background event rate means that the padlock probes themselves cannot be detected by the pore due to their small size. In contrast, for the positive reactions (three right traces), clear blockage events were observed (Figure S3 shows representative single translocation event profiles). The exponential distribution of the interarrival time between events (Figure S4) indicates that the translocation events follow a Poisson process, which means that the translocations are random and independent.[27] Further analysis of these events revealed that the elongated amplicons for let-7a, miR-30e, and miR-21 were similar in their size distribution because their dwell time and peak current are comparable (Figure 1d). This is consistent with the gel results shown in Figure 1b. Given the similar size of starting ligated products for let-7a, miR-30e, and miR-21 (Figure 1a), we indeed expect the ssDNA amplicons to be comparable in size after the same duration of RCA elongation.

While the dwell time versus peak current distributions were comparable for let-7a, miR-30e, and miR-21 products, it is also evident that their event rate differed from each other (Figure 1e). This is because we intentionally used different quantities of these three miRNAs. We used 80 fmol of let-7a, 40 fmol of miR-30e, and 20 fmol of miR-21, together with 160 fmol of their corresponding padlock probes for the RCA reactions.

https://doi.org/10.1021/acs.analchem.1c04781
Anal. Chem. 2022, 94, 3865−3871

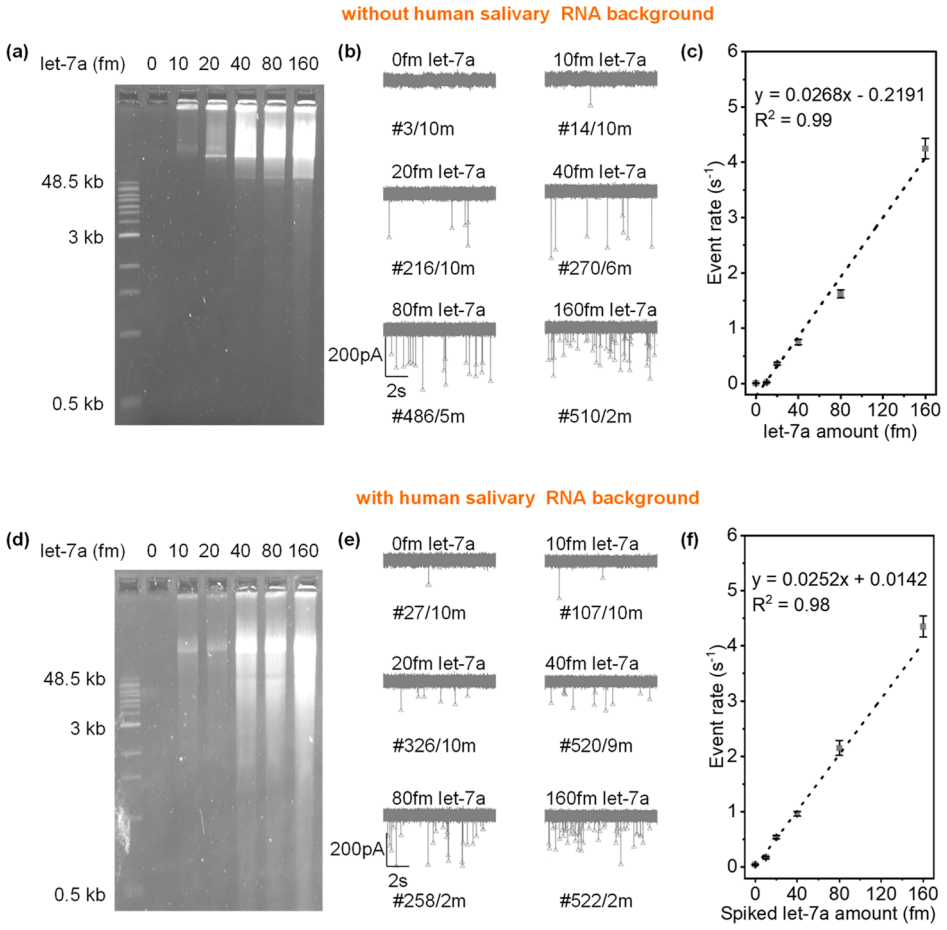

Figure 2. (a) Gel image of the RCA products with different quantities of the purified let-7a (without human salivary total RNA). (b) Corresponding current traces obtained in nanopore sensing. (c) Extracted event rate as a function of the let-7a quantity. The error bars represent the Poisson rate uncertainty. (d) Gel image of the RCA products with different let-7a quantities in the salivary total RNA background. (e) Corresponding current traces obtained in nanopore sensing with salivary total RNA background. (f) Extracted nanopore event rate as a function of the let-7a quantity with salivary total RNA background.

Please note that we reported the miRNA quantity instead of the concentration throughout this work to avoid the possible confusion caused by the varying volumes of RCA buffers and nanopore measurement buffers. To examine if the measured amplicon event rate is quantitatively correlated to the miRNA concentration, we extracted the event rate for each of these samples and plotted it against the initial miRNA concentration (Figure 1e). As shown, there is an excellent correlation between the miRNA concentration and the nanopore event rate (R^2 = 0.99). This linear correlation suggested that inter-miRNA profiling is feasible by the RCA-coupled glass nanopore counting platform.

Quantification of miRNAs with and without Salivary RNA Background. Previous studies have shown that mTBI-related miRNAs could increase 2 times for positive patients.[21−24] To further evaluate the intra-miRNA quantification ability of the RCA-coupled nanopore counting platform, we prepared a 2× serial dilution of let-7a miRNAs and performed 30 min of RCA reaction with let-7a quantities ranging from 0 to 160 fmol (corresponding to the clinically relevant miRNA concentration range of 0−160 pM[28] with 1 mL of raw saliva sample). The resulting RCA products were examined with gel (Figure 2a). As shown, the RCA product concentration increases when the input let-7a miRNAs increases. This is not surprising as the padlock probes were excessively provided in all reactions. To quantify these RCA products, we performed the nanopore counting experiment. The representative 10 s current traces at different let-7a quantities are shown in Figure 2b. The background event rate observed for reactions without let-7a input was less than 0.005 s^{-1} (Figure S5a). The event rate went from 0.023 s^{-1} with 10 fmol let-7a to 4.250 s^{-1} with 160 fmol let-7a. Figure 2c summarizes the correlation between the measured event rate and the initial let-7a quantity. A linear relationship with R^2 of 0.99 was observed, suggesting that the nanopore event rate of the amplicons is an excellent measurement of the initial miRNA concentrations.

To further test if the salivary total RNA background would interfere with the nanopore counting, different concentrations of the purified let-7a were spiked into the salivary RNA background. We performed 30 min of RCA elongation with these spiked samples (in which let-7a quantities range from 0 to 160 fmol and the padlock probe is 160 fmol). Figure 2d presents the gel results from these reactions. Similar to the case without salivary RNA background (Figure 2a), more input let-7a produced an increased amount of RCA amplicons with salivary RNA background. We also performed the nanopore counting on these RCA products. Figure 2e presents the representative current traces. As expected, more translocation events were observed as more let-7a miRNAs were spiked.

https://doi.org/10.1021/acs.analchem.1c04781
Anal. Chem. 2022, 94, 3865−3871

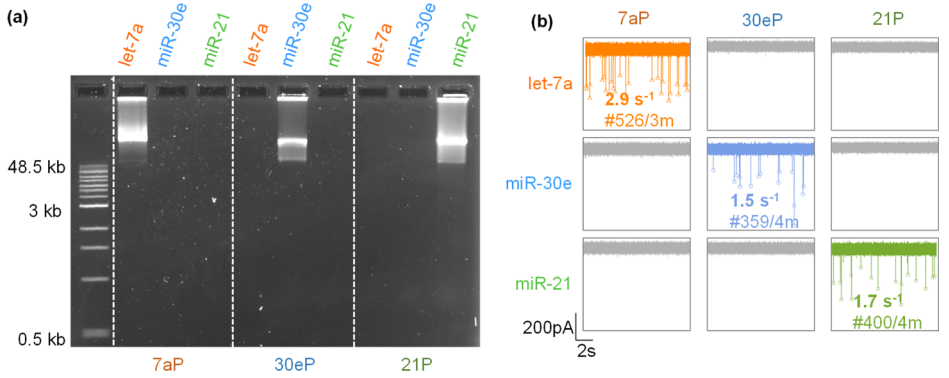

Figure 3. (a) Gel image of RCA products for different combinations of miRNAs and padlock probes. Each RCA reaction was performed with 160 fmol probes and 40 fmol miRNAs. (b) Corresponding current traces for each miRNA and padlock combination. Evident events were visible only in the specific combinations.

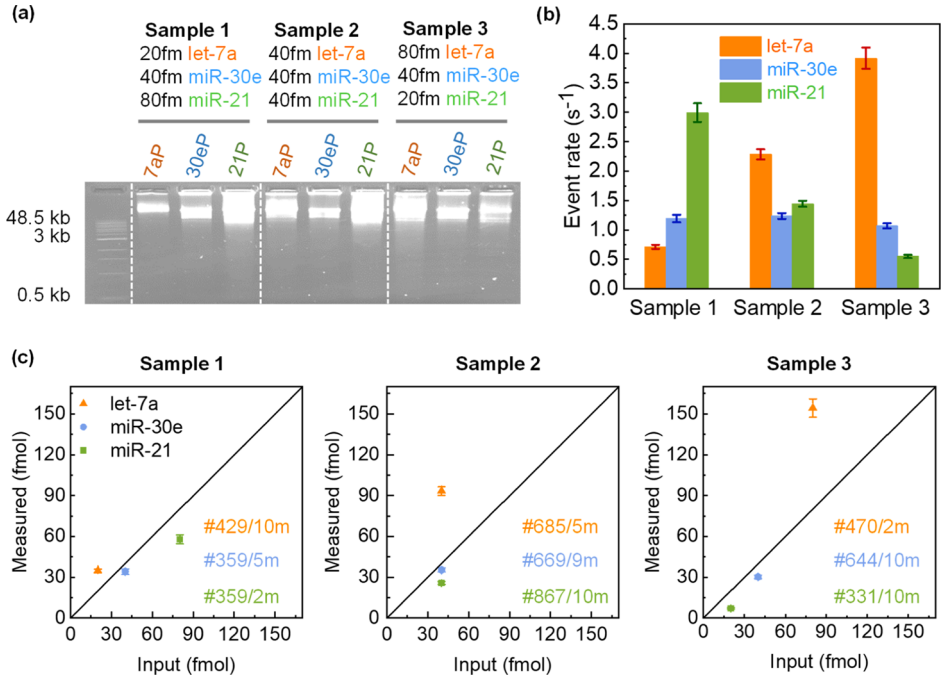

Figure 4. (a) Gel image of the RCA products for three mixed samples with varying quantities of let-7a, miR-30e, and miR-21. Sample 1 contains 20 fmol let-7a, 40 fmol miR-30e, and 80 fmol miR-21; sample 2 contains 40 fmol let-7a, 40 fmol miR-30e, and 40 fmol miR-21; sample 3 contains 80 fmol let-7a, 40 fmol miR-30e, and 20 fmol miR-21. Each of these mock samples was parallelly reacted with a specific padlock probe. (b) Measured event rates for each of the three mixed samples. (c) Measured individual miRNA concentration vs the input miRNA concentration for each of three mixed samples. The solid line denotes the expected value. The error bars represent the Poisson uncertainty.

Figure 2f plots the event rate as a function of the initial let-7a quantity spiked into the salivary RNA background. As shown, there is also an excellent linear relationship with R^2 of 0.98. Interestingly, the event rate at each let-7a concentration is slightly higher with salivary RNA background than that without it. For example, the event rate observed for reactions of 0 fmol let-7a input was 0.045 and 0.005 s^{-1} with and without salivary RNA background, respectively (Figure S5a,b). This increased background event rate is likely due to the RCA amplicons of the preexisting let-7a in the extracted salivary RNAs rather than the salivary RNAs themselves. In fact, the gel analysis revealed that the size range of the extracted salivary RNA is shorter than 500 nucleotides (Figure S5d). These smaller sized background RNAs are too small to be detected by our pores with 200 nm diameter (Figure S5c). The quantification experiments of miR-30e and miR-21 were also performed (Figures S6 and S7).

Specificity of RCA-Coupled Nanopore Counting. Due to the short length and high homogeneity of miRNAs, the specificity of designed padlock probes is vital for accurate miRNA identification and quantification.[11,18] To evaluate the specificity of our padlock probes against let-7a, miR-30e, and miR-21, we performed the cross-reactivity test by running nine RCA reactions with different miRNA/probe combinations. The resulting amplicons were examined by gel analysis (Figure 3a). As shown, no bands were observed for the nonspecific combinations. Only the combinations of miRNA and its specific probe could produce the elongated RCA products with a size larger than 48.5 kb. These RCA products were subsequently analyzed by the glass sub-micron pore sensor. Figure 3b plots the representative current traces for each case

https://doi.org/10.1021/acs.analchem.1c04781
Anal. Chem. 2022, 94, 3865−3871

(under 400 mV bias voltage). As expected, translocation events with a rate larger than 1 s^{-1} were evident for the specific reactions, whereas the event rates were negligible for the nonspecific reactions (<0.003 s^{-1}; see Figure S8). There is a significant event rate difference between the specific reaction and the nonspecific reaction. This means that the designed padlock probes are specific to their targets and there is no cross-reactivity among the panel members of let-7a, miR-30e, and miR-21. In addition, the sub-micron pore sensor is responsive only to the specifically elongated ssDNAs without interference from the background molecules from RCA reactions.

Profiling mTBI-Related miRNAs from a Mixture. Recent studies have shown that a panel of multiple miRNAs represents a more accurate biomarker for mTBI.[7,21,22,24,29,30] To evaluate the ability of the RCA-coupled nanopore counting platform to profile multiple miRNAs in a mixture, we carried out the quantification experiment using a mixture solution containing varying amounts of let-7a, miR-30e, and miR-21. The relative abundance of each of these miRNAs was intentionally controlled. A total of three samples were tested (Figure 4a). As shown in the gel images, there were clear RCA products for each of these mixture samples added into a specific probe, indicating the success of the RCA assay for the mixed samples.

We then performed the nanopore counting to quantify the miRNA constitutes. Figure 4b plots the event rates for different miRNAs in each of these mixed samples. As can be seen, the event rates for miR-30e were consistent among these samples due to the same miRNA quantity (40 fmol). The relative event rates profile for let-7a and miR-21 from samples 1 to 3 qualitatively agree with the input let-7a quantity in these samples. To test the quantitative agreement between the input and the output, we used the correlation equation obtained in Figures 2c, S6, and S7 to convert the event rate into the concentration. Figure 4c presents the measured miRNA quantity versus the input miRNA quantity for three samples. A line with a slope of 1 was overlaid with the plot, representing an ideal measurement. As can be seen, while not all the data points fall on the ideal line, the measured quantity agrees very well with the input quantity. The relative abundance of let-7a, miR-30e, and miR-21 in each of these mixed samples was correctly captured.

To understand the factors that lead to the measurement uncertainty, one can examine the event rate versus the analyte concentration relationship in nanopore counting. Previous work shows that the capture of 48.5 kbp DNA is diffusion-limited when using 10 nm glass nanopore.[26] Because the glass nanopores used in our experiments are around 200 nm in diameter, they are large enough such that the transport is diffusion-limited rather than barrier-limited. It was known that the event rate can be linked to the analyte concentration C in the diffusion-limited region as $R = 2\pi\mu d\Delta VC$,[31] in which μ is the free solution electrophoretic mobility, ΔV is the applied electric potential across the pore, and d is the characteristic length of the pore. The analyte (RCA amplicons) concentration C can be linked to the miRNA concentration C_0 as $C = \alpha C_0 T_r$, in which α is the reaction efficiency and T_r is the reaction time. In our experiments, we used the same 0.4 V bias voltage for all measurements; therefore, ΔV would not contribute to the variations. In addition, the free solution electrophoretic mobility of DNA in the Tris-EDTA buffer was shown to be independent of the DNA length longer than 400 bp;[32] the contribution of the RCA product mobility to the event rate measurement can also be ruled out. Given the same reaction time T_r, the measurement uncertainty is most likely due to the variations in nanopore characteristic length d and RCA reaction efficiency α. While all the nanopore devices we tested have a comparable aperture (217 ± 9 nm), their actual geometry (characteristic length d) could be different. Therefore, the event rate counted by each device could be different. On the other hand, the RCA reaction efficiency α could vary between different miRNAs. This is consistent with previous observations that the hybridization,[33] ligation,[34] and elongation[35] efficiency could vary for different miRNAs and probe combinations. Although the event rate variations exist, they do show a good linear relationship (R^2 > 97%) with input miRNA quantities when counting by a single nanopore device (Figures 2, S6, and S7). Therefore, we use the same nanopore device to count both healthy and patient miRNAs to more accurately compare the population via event rate in our future work.

CONCLUSIONS

In summary, we developed an RCA-coupled resistive pulse counting platform for profiling mTBI-related salivary miRNAs using low-cost and easy-to-fabricate large glass nanopores (200 nm diameter). We developed and validated the RCA assays, which showed an excellent specificity for target miRNAs. We showed that miRNA quantity has a good linear relationship with the nanopore event rate in the range of 0−160 fmol, which corresponds to the clinically relevant miRNA concentration range of 0−160 pM with 1 mL of raw saliva sample.[28] In addition, the RCA-coupled large glass nanopore counting platform has a resolution of 2× for miRNA quantification, which is sufficient to resolve typical mTBI-related miRNA changes for positive patients.[21−24] The RCA-coupled nanopore counting platform was shown to be capable of profiling a panel of let-7a, miR-30e, and miR-21 miRNAs in a mixed analyte. Due to the scalability of the electronics, our nanopore counting platform could easily accommodate more miRNA panel members as compared to the conventional gel analysis. With less than 2 h of turnaround time and a relatively simple workflow, we believe that the RCA-coupled large glass nanopore counting platform provides a promising alternative toward the clinical diagnosis of mTBI using salivary miRNAs.

ASSOCIATED CONTENT

Supporting Information

The Supporting Information is available free of charge at https://pubs.acs.org/doi/10.1021/acs.analchem.1c04781.

Characterization of glass sub-micron pore, current traces for the probe-only reactions, typical RCA product translocation events, normalized distributions of inter-arrival time for different miRNAs, current traces of the 0 fmol let-7a RCA assay without and with total RNA background, current traces and gel image of the extracted salivary RNA without RCA assay, quantification of miR-30e, quantification of miR-21, current traces of the nonspecific reactions, and miRNA and padlock probe sequences used in this study (PDF)

AUTHOR INFORMATION

Corresponding Author

Weihua Guan − *Department of Electrical Engineering and Department of Biomedical Engineering, Pennsylvania State*

https://doi.org/10.1021/acs.analchem.1c04781
Anal. Chem. 2022, 94, 3865−3871

University, University Park, Pennsylvania 16802, United States; orcid.org/0000-0002-8435-9672; Phone: 1-814-867-5748; Email: w.guan@psu.edu

Authors

Ming Dong − *Department of Electrical Engineering, Pennsylvania State University, University Park, Pennsylvania 16802, United States*

Zifan Tang − *Department of Electrical Engineering, Pennsylvania State University, University Park, Pennsylvania 16802, United States*

Steven Hicks − *Department of Pediatrics, Penn State College of Medicine, Hershey, Pennsylvania 17033, United States*

Complete contact information is available at: https://pubs.acs.org/10.1021/acs.analchem.1c04781

Author Contributions

W.G. conceived the concept and supervised the study. M.D. developed and validated the RCA assay and performed glass nanopore quantification experiments. Z.T. developed the nanopore sensing protocols. S.H. provided the miRNA panels related to mTBI. W.G. and M.D. co-wrote the manuscript and discussed it with all other authors.

Notes

The authors declare no competing financial interest.

■ ACKNOWLEDGMENTS

This work supported by the National Science Foundation under grant no. 2045169. Any opinions, findings, and conclusions or recommendations expressed in this work are those of the authors and do not necessarily reflect the views of the National Science Foundation. W.G. and S.H. acknowledge the support of the Penn State Center for Biodevices Seed Grant.

■ REFERENCES

(1) Voss, J. D.; Connolly, J.; Schwab, K. A.; Scher, A. I. *Curr. Pain Headache Rep.* **2015**, *19*, 32.
(2) Davis, G. A.; Iverson, G.; Guskiewicz, K.; Ptito, A.; Johnston, K. *Br. J. Sports Med.* **2009**, *43*, i36−i45.
(3) Gosselin, N.; Bottari, C.; Chen, J.-K.; Huntgeburth, S. C.; De Beaumont, L.; Petrides, M.; Cheung, B.; Ptito, A. *Neurosurg. Focus* **2012**, *33*, No. E7.
(4) Papa, L.; Ramia, M. M.; Kelly, J. M.; Burks, S. S.; Pawlowicz, A.; Berger, R. P. *J. Neurotrauma* **2013**, *30*, 324−338.
(5) Bazarian, J. J.; Zemlan, F. P.; Mookerjee, S.; Stigbrand, T. *Brain Inj.* **2006**, *20*, 759−765.
(6) Posti, J. P.; Hossain, I.; Takala, R. S. K.; Liedes, H.; Newcombe, V.; Outtrim, J.; Katila, A. J.; Frantzén, J.; Ala-Seppälä, H.; Coles, J. P.; Kyllönen, A.; Maanpää, H.-R.; Tallus, J.; Hutchinson, P. J.; van Gils, M.; Menon, D. K.; Tenovuo, O. *J. Neurotrauma* **2017**, *34*, 1427−1438.
(7) Hicks, S. D.; Olympia, R. P.; Onks, C.; Kim, R. Y.; Zhen, K. J.; Fedorchak, G.; DeVita, S.; Rangnekar, A.; Heller, M.; Zwibel, H.; Monteith, C.; Gagnon, Z.; McLoughlin, C. D.; Randall, J.; Madeira, M.; Campbell, T. R.; Fengler, E.; Dretsch, M. N.; Neville, C.; Middleton, F. A. *Int. J. Mol. Sci.* **2020**, *21*, 7758.
(8) Ambros, V. *Nature* **2004**, *431*, 350−355.
(9) Leshkowitz, D.; Horn-Saban, S.; Parmet, Y.; Feldmesser, E. *RNA* **2013**, *19*, 527−538.
(10) Válóczi, A.; Hornyik, C.; Varga, N.; Burgyán, J.; Kauppinen, S.; Havelda, Z. *Nucleic Acids Res.* **2004**, *32*, No. e175.
(11) Chen, C.; Ridzon, D. A.; Broomer, A. J.; Zhou, Z.; Lee, D. H.; Nguyen, J. T.; Barbisin, M.; Xu, N. L.; Mahuvakar, V. R.; Andersen, M. R. *Nucleic Acids Res.* **2005**, *33*, No. e179.
(12) Li, W.; Ruan, K. *Anal. Bioanal. Chem.* **2009**, *394*, 1117−1124.
(13) Weisz, H. A.; Kennedy, D.; Widen, S.; Spratt, H.; Sell, S. L.; Bailey, C.; Sheffield-Moore, M.; DeWitt, D. S.; Prough, D. S.; Levin, H.; Robertson, C.; Hellmich, H. L. *Sci. Rep.* **2020**, *10*, 3341.
(14) Koscianska, E.; Starega-Roslan, J.; Czubala, K.; Krzyzosiak, W. J. *Sci. World J.* **2011**, *11*, 102−117.
(15) Hwang, D. W.; Song, I. C.; Lee, D. S.; Kim, S. *Small* **2010**, *6*, 81−88.
(16) Li, F.; Peng, J.; Wang, J.; Tang, H.; Tan, L.; Xie, Q.; Yao, S. *Biosens. Bioelectron.* **2014**, *54*, 158−164.
(17) Deng, R.; Zhang, K.; Li, J. *Acc. Chem. Res.* **2017**, *50*, 1059−1068.
(18) Cheng, Y.; Zhang, X.; Li, Z.; Jiao, X.; Wang, Y.; Zhang, Y. *Angew. Chem.* **2009**, *121*, 3318−3322.
(19) Wanunu, M.; Dadosh, T.; Ray, V.; Jin, J.; McReynolds, L.; Drndić, M. *Nat. Nanotechnol.* **2010**, *5*, 807−814.
(20) Wang, Y.; Zheng, D.; Tan, Q.; Wang, M. X.; Gu, L.-Q. *Nat. Nanotechnol.* **2011**, *6*, 668−674.
(21) Svingos, A. M.; Asken, B. M.; Bauer, R. M.; DeKosky, S. T.; Hromas, G. A.; Jaffee, M. S.; Hayes, R. L.; Clugston, J. R. *Brain Inj.* **2019**, *33*, 1−7.
(22) Hicks, S. D.; Johnson, J.; Carney, M. C.; Bramley, H.; Olympia, R. P.; Loeffert, A. C.; Thomas, N. J. *J. Neurotrauma* **2018**, *35*, 64−72.
(23) Harrison, E. B.; Hochfelder, C. G.; Lamberty, B. G.; Meays, B. M.; Morsey, B. M.; Kelso, M. L.; Fox, H. S.; Yelamanchili, S. V. *FEBS Open Bio* **2016**, *6*, 835−846.
(24) Atif, H.; Hicks, S. D. *J. Exp. Neurosci.* **2019**, *13*, 1179069519832286.
(25) Blanco, L.; Bernad, A.; Lázaro, J. M.; Martín, G.; Garmendia, C.; Salas, M. *J. Biol. Chem.* **1989**, *264*, 8935−8940.
(26) Nouri, R.; Tang, Z.; Guan, W. *Anal. Chem.* **2019**, *91*, 11178−11184.
(27) Meller, A.; Branton, D. *Electrophoresis* **2002**, *23*, 2583−2591.
(28) Tavallaie, R.; De Almeida, S. R. M.; Gooding, J. J. *Wiley Interdiscip. Rev.: Nanomed. Nanobiotechnol.* **2015**, *7*, 580−592.
(29) Di Pietro, V.; Porto, E.; Ragusa, M.; Barbagallo, C.; Davies, D.; Forcione, M.; Logan, A.; Di Pietro, C.; Purrello, M.; Grey, M.; Hammond, D.; Sawlani, V.; Barbey, A. K.; Belli, A. *Front. Mol. Neurosci.* **2018**, *11*, 290.
(30) Di Pietro, V.; O'Halloran, P.; Watson, C. N.; Begum, G.; Acharjee, A.; Yakoub, K. M.; Bentley, C.; Davies, D. J.; Iliceto, P.; Candilera, G.; Menon, D. K.; Cross, M. J.; Stokes, K. A.; Kemp, S. P.; Belli, A. *Br. J. Sports Med.* **2021**, *55*, 1395.
(31) Chen, P.; Gu, J.; Brandin, E.; Kim, Y.-R.; Wang, Q.; Branton, D. *Nano Lett.* **2004**, *4*, 2293−2298.
(32) Stellwagen, E.; Stellwagen, N. C. *Electrophoresis* **2002**, *23*, 2794−2803.
(33) Xu, S.; Zhan, J.; Man, B.; Jiang, S.; Yue, W.; Gao, S.; Guo, C.; Liu, H.; Li, Z.; Wang, J. *Nat. Commun.* **2017**, *8*, 14902.
(34) Zhang, Z.; Lee, J. E.; Riemondy, K.; Anderson, E. M.; Yi, R. *Genome Biol.* **2013**, *14*, R109.
(35) Lee, S. Y.; Kim, K.-R.; Bang, D.; Bae, S. W.; Kim, H. J.; Ahn, D.-R. *Biomater. Sci.* **2016**, *4*, 1314−1317.